

PARTICLE-IN-CELL SIMULATIONS OF THE TWISTED MAGNETOSPHERES OF MAGNETARS

ALEXANDER Y. CHEN, ANDREI M. BELOBORODOV

Physics Department and Columbia Astrophysics Laboratory, Columbia University, 538 West 120th Street New York, NY 10027

Draft version November 1, 2016

ABSTRACT

The magnetospheres of magnetars are believed to be filled with electron-positron plasma generated by electric discharge. We present a first direct numerical experiment showing how the plasma is created in an axisymmetric closed magnetosphere. The e^\pm discharge occurs in response to twisting of the magnetic field lines by a shear deformation of the magnetar surface, which launches electric currents into the magnetosphere. The simulation shows the formation of an electric “gap” with unscreened electric field ($\mathbf{E} \cdot \mathbf{B} \neq 0$) that continually accelerates particles along the magnetic field lines and sustains pair creation. The accelerating voltage is self-regulated to the threshold of the e^\pm discharge. It controls the rate of energy release and the lifetime of the magnetic twist. The simulation follows the global evolution of the twisted magnetosphere over a long time and demonstrates its gradual resistive untwisting. A vacuum cavity forms near the star and expands, gradually erasing magnetospheric electric currents j . The active j -bundle shrinks with time and its footprints form shrinking hot spots on the magnetar surface bombarded by the created particles.

Subject headings: stars: magnetars — magnetic fields — plasmas — relativistic processes

1. INTRODUCTION

Magnetars are neutron stars with ultrastrong magnetic fields ($B \gtrsim 10^{14}$ G) that display strong activity fed by dissipation of magnetic energy (see e.g. Mereghetti 2008; Turolla et al. 2015 for reviews). They produce strong outbursts and flares as well as bright persistent emission with a prominent hard X-ray component extending above 100 keV. These activities are associated with strong deformations of the external magnetosphere of the neutron star, resembling the activity of the solar corona (e.g. Thompson & Duncan 1995). The magnetosphere is anchored in the solid crust of the star and its deformation is caused by crustal shear motions driven by ultrastrong internal magnetic stresses.

The speed of the surface motions is poorly known. Recent work suggests that the crust yields to internal stresses through an instability launching a thermoplastic wave (Beloborodov & Levin 2014) or a Hall-mediated avalanche (Li et al. 2016). In both cases the motion is plastic and should occur on a timescale much longer than the Alfvén crossing timescale (10–100 ms). It is expected to be fast enough to efficiently twist the external magnetosphere.

The surface shear motion launches Alfvén waves along the magnetic field lines and generates magnetospheric twist $\nabla \times \mathbf{B} \neq 0$ (Thompson et al. 2002; Parfrey et al. 2013, hereafter PBH13). Plasma is required to supply the current $\mathbf{j} = (c/4\pi)\nabla \times \mathbf{B}$. Beloborodov & Thompson (2007, hereafter BT07) found that plasma must be mainly supplied through e^\pm discharge in the magnetosphere rather than through extraction of charges from the star. They performed simplified one-dimensional (1D) simulations of the discharge. In the simulations, the magnetosphere was replaced by a fixed, uniform field $\mathbf{B}(x)$ connecting anode and cathode — metallic plates at x_A and x_C . The fixed $\nabla \times \mathbf{B}$ in this setup turns out equivalent to imposing an electric current through the

plates into the computational box. When pair creation was not allowed, the system quickly relaxed to a global “double layer” configuration, with surface charges of the opposite sign induced on the plates. The electric field between them gave a huge voltage Φ_e accelerating particles to ultra-high energies. When pair creation process was included in the simulation, the voltage dropped to a much lower value, just sufficient to sustain pair creation, and the current was supported through continual e^\pm discharge. BT07 concluded that pair creation must be responsible for screening electric fields and regulating the magnetospheric activity of magnetars.

The simplified 1D model cannot, however, give a complete picture of the magnetospheric activity, for a few reasons. It does not show how $\nabla \times \mathbf{B}$ is imparted in the first place, as the 1D model does not support Alfvén waves. The exclusion of this important degree of freedom may also put in question the double layer formation in the absence of pair creation, the necessity of the onset of pair creation, and the self-regulation of the discharge voltage seen in the 1D model. Note also that the electric field in the 1D (slab) geometry does not decrease with distance from the charge, and hence one cannot see a realistic distribution of the accelerating electric field along the magnetospheric field lines. Finally, the 1D model offers no way to follow the gradual resistive “untwisting” of the magnetosphere — its global evolution as a result of ohmic dissipation of the twist energy. The expected evolution must occur on the resistive timescale of months to years (regulated by voltage Φ_e) and can be tested against observations.

An axisymmetric electrodynamic model of a resistively untwisting magnetosphere was developed by Beloborodov (2009, hereafter B09). This model assumed that a given fixed voltage Φ_e is sustained on current-carrying field lines, without calculating the discharge that regulates Φ_e . A surprising result was the formation of two distinct regions in the untwisting magneto-

sphere, with a sharp boundary between them, — a “cavity” ($j = 0$) and a “j-bundle.” In essence, the untwisting process was found to be the growth of the cavity, erasing the currents in the j-bundle. A curious immediate implication was the prediction of shrinking hot spots on magnetars — the footprints of the shrinking j-bundle, where the stellar surface is heated by bombardment of accelerated particles. Shrinking hot spots have been observed in seven objects by now (see data compilation in Beloborodov & Li 2016). All of these objects belong to the class of “transient magnetars” that show a sudden outburst and then gradually decay back to the quiescent state of low luminosity. A key parameter governing the j-bundle evolution is its poorly known voltage Φ_e , which depends on how the e^\pm discharge is self-organized and may be different on different magnetospheric field lines.

The goal of the present paper is to overcome the limitations of the 1D discharge model and perform a first self-consistent calculation of the e^\pm discharge in an axisymmetric twisted magnetosphere. The process can be simulated from first-principles using a full kinetic description of the magnetospheric plasma as a large number of charged particles moving in the self-consistent collective electromagnetic field. Such a direct numerical experiment will show how the twist and the electric current are created in the magnetosphere in response to crustal shear, and will follow the ensuing dissipative evolution of the twist.

The self-organization of the e^\pm discharge should determine where the particles are created and accelerated. Should this occur near the footpoints of the magnetospheric field line or near its apex? Will the acceleration region be steady or move around? Answers to these questions may have important implications for nonthermal emission from magnetars. The voltage drop along the twisted field lines will control the dissipated power which feeds the observed emission. We expect to see how particles are accelerated in the current-carrying magnetic loop and rain down on the stellar surface to create hotspots. Finally, the established discharge voltage will determine the life-time of the magnetic twist and the pattern of its evolution.

A suitable technique for such direct numerical experiments is the particle-in-cell (PIC) method, with pair creation implemented. This method has been successfully applied to the old problem of rotation-powered pulsars (Chen & Beloborodov 2014, hereafter CB14; Philippov et al. 2015; Belyaev 2015; Cerutti et al. 2016) The magnetar problem is different in important ways and in some ways easier to study using a global PIC simulation, as will be described below.

The paper is organized as follows. In Section 2 we describe the theory of twisted magnetospheres in axisymmetric geometry, revisit the double-layer configuration (in the absence of pair creation), describe the mechanism of pair creation and basic electrodynamics of untwisting. This will be useful for understanding the simulation results and also introduces notation used in the paper. Section 3 presents the setup of our numerical experiments. Section 4 describes the results and their implications. Finally in Section 5 we summarize our conclusions and provide an outlook for future studies.

2. SUSTAINING CURRENTS IN THE TWISTED MAGNETOSPHERE

Let us consider a dipole magnetic field around the star, and assume that its footpoints on the star are sheared in the azimuthal direction about the magnetic axis. In this case, the implanted twist is axisymmetric and its amplitude ψ is simply given by the azimuthal angle between the two footpoints of the magnetic field line. It is convenient to use spherical coordinates r, θ, ϕ with the polar axis being the axis of symmetry. The magnetospheric twist implies a toroidal component of the magnetic field $B_\phi \neq 0$, and the twist amplitude on a given magnetic field line is related to B_ϕ by

$$\psi = \int_p^q \frac{B_\phi}{B r \sin \theta} d\ell, \quad (1)$$

where the integral is taken along the field line, and p, q are the two footpoints where the field line is anchored to the surface. As long as the implanted twist ψ is smaller than unity, the poloidal magnetic field remains close to dipolar, and the deformation can be thought of as simply adding a toroidal component B_ϕ without changing the poloidal dipole component (B_{09}). This induces $\nabla \times \mathbf{B}$ in the dipolar configuration that was originally curl-free. It must be sustained by an electric current in the magnetosphere, \mathbf{j} . The magnetic energy strongly dominates over the plasma energy, and hence the currents must be nearly force-free, $\mathbf{j} \times \mathbf{B} = 0$, i.e. flowing along the magnetic field lines.

The origin of the plasma that could carry the current is a non-trivial issue. The star can have a gaseous atmosphere, however for the typical surface temperature $kT < 1$ keV the atmosphere scale-height is tiny (centimeters), because of the strong gravity of the neutron star. The atmosphere does not provide enough plasma to conduct currents at large altitudes $r \sim R_*$, where $R_* = 10 - 13$ km is the neutron star radius.

Spinning of the neutron star and its magnetosphere with velocity $\mathbf{v}_{\text{rot}} = \boldsymbol{\Omega} \times \mathbf{r}$ implies a “co-rotation” electric field $\mathbf{E} = -\mathbf{v}_{\text{rot}} \times \mathbf{B}/c$ and requires charge density $\rho_{\text{GJ}} = \nabla \cdot \mathbf{E}/4\pi = -\boldsymbol{\Omega} \cdot \mathbf{B}/2\pi c$ (Goldreich & Julian 1969). Magnetars are slow rotators, $\Omega \sim 1$ Hz, and their ρ_{GJ} is small. The currents demanded by the twisted magnetosphere are typically much stronger than $c\rho_{\text{GJ}}$.

The magnetosphere must make a special effort to avoid charge starvation and create sufficiently dense plasma to conduct the current \mathbf{j} demanded by the twist. It achieves this by inducing an electric field E_{\parallel} (parallel to the magnetic field lines) that can accelerate particles and trigger pair creation. This implies a finite voltage in the magnetospheric electric circuit and a finite rate of ohmic dissipation.

2.1. Voltage without pair discharge

In the absence of pair creation, the star is the only available source of magnetospheric plasma. The lack of charges leads to induction of an electric field with a component parallel to the magnetic field, which can pull out charges from the star and accelerate them. Then the electric circuit is expected to relax to a static configuration similar to the relativistic double layer derived by Carlqvist (1982) and observed in the 1D plasma simulations of BT07. It sustains the opposite surface charges at the

two footpoints of the magnetic loop where the lifted particles still move slowly, $v \ll c$, and create a large charge density $\rho \sim j/v$.

The high charge density near the footpoints generates E_{\parallel} according to the Gauss law, and E_{\parallel} accelerates the flow on the plasma timescale $\omega_p^{-1} = (m_e/4\pi e\rho)^{1/2}$. The flow density ρ is reduced to its minimum where its velocity approaches c . As a result, the characteristic thickness of the surface charge layer is the plasma skin depth $\lambda_p = c/\omega_p$ evaluated for the plasma density $\rho \sim j/c$.

The surface charge $\Sigma \sim (j/c)\lambda_p$ generates the self-consistent electric field that lifts and accelerates particles from the footpoint,

$$E_{\parallel} \sim 4\pi\rho\lambda_p \sim \frac{4\pi j}{\omega_p}, \quad (2)$$

where ω_p is the plasma frequency defined by

$$\omega_p^2 = \frac{4\pi e\rho}{m_e}, \quad \rho = \frac{j}{c}. \quad (3)$$

In other words, the surface charge near the anode and cathode is organized so that particles extracted from the star are accelerated to $v \sim c$ over a length comparable to the plasma skin depth.

For simplicity, consider a symmetric double layer where the positive and negative charges have the same mass. In the 1D model, the electric field is almost constant between the two surface charges of the double layer, giving a voltage drop,

$$\frac{e\Phi_e}{m_e c^2} = \frac{4\pi j e L}{\omega_p m_e c^2} = \frac{\omega_p L}{c} = \frac{L}{\lambda_p}, \quad (4)$$

where L is the size of the layer (the distance between the footpoints). Using $j \sim \psi B/L$, one finds for the typical parameters of a magnetar,

$$\frac{L}{\lambda_p} \sim 10^8 L_6^{3/2} \psi^{-1/2} B_{15}^{-1/2}, \quad (5)$$

which implies a huge voltage Φ_e .

The estimate in Equation (4) is not valid, however, for a realistic magnetosphere, which is not one-dimensional. The current flows along the curved magnetic field lines and their dipolar geometry significantly changes the distribution of the net voltage sustained between the two footpoints.

The corrected voltage may be estimated as follows. Since λ_p is small compared with the thickness of the j-bundle, the surface charge remains thin and its structure is not changed from the 1D model. The self-consistent electric field extracting charges from the footpoint is still described by Equation (2). However, with increasing altitude the electric field must be reduced on a scale comparable to the horizontal size of surface charge W (thickness of the j-bundle). The resulting potential drop saturates at $\Phi_e \sim E_{\parallel} W$, which gives

$$\gamma_{\text{DL}} = \frac{e\Phi_e}{m_e c^2} \sim \frac{W}{\lambda_p}. \quad (6)$$

It is smaller than the 1D estimate by the factor of W/L . For instance a j-bundle of thickness $W \sim 0.1R_{\star}$ at the

stellar surface and length $L \sim 10R_{\star}$ would sustain a voltage $\sim 10^{-2}$ smaller than predicted by the 1D model. This is still a huge voltage and particles that tap the full potential drop will be able to induce pair discharge, making the double layer model inconsistent.

One should also note that $E_{\parallel} = \mathbf{E} \cdot \mathbf{B}/B$, and hence the voltage,

$$\Phi_e = \int_p^q E_{\parallel} dl, \quad (7)$$

have a pure inductive origin. One should think of E_{\parallel} as $c^{-1}\partial A_{\parallel}/\partial t$, the result of the slow decay of the ultra-strong twisted magnetic field (BT07). $e\Phi_e$ measures the energy gain of charge e completing the electric circuit, and this released energy is extracted from the magnetic twist energy. A potential electric field would be unable to support any significant voltage between the footpoints, as they are connected by an excellent conductor — the crust.

The induction electric field \mathbf{E} still satisfies the Gauss law $\nabla \cdot \mathbf{E} = 4\pi\rho$; as long as the untwisting process occurs much slower than the light crossing of the system, one can think of the dissipation as a quasi-steady process. The inductive double layer is similar to a normal electrostatic double layer except that the integral of \mathbf{E} along the full closed circuit (including the part closing through the crust, where $\mathbf{E} = 0$) does not vanish and instead equals Φ_e . There is no external emf applied to the circuit below the stellar surface; the only emf sustaining the current is the induction emf due to the twist decay in the magnetosphere itself.

2.2. Voltage with pair discharge

The mechanism of secondary e^{\pm} creation by relativistic particles in the magnetar magnetosphere involves an intermediate step of gamma-ray production. It occurs through resonant Compton scattering of photons flowing from the star by particles accelerated in the magnetosphere. A target photon with energy $E_t \sim 1$ keV can be resonantly scattered by an electron with Lorentz factor γ if the photon energy measured in the electron rest frame matches $\hbar\omega_B$, where $\omega_B = eB/m_e c$.¹ The resonance condition reads

$$\gamma(1 - \beta \cos \theta_X) E_t = \hbar\omega_B, \quad (8)$$

where θ_X is the angle of the target X-ray with respect to local magnetic field line (the electron moves along the field line). The energy $\hbar\omega_B$ equals $m_e c^2$ for the characteristic magnetic field $B_Q = m_e^2 c^3 / e\hbar \approx 4.4 \times 10^{13}$ G and scales linearly with B .

Magnetars supply plenty of keV photons, and the electron Lorentz factor required for resonant scattering at $B \sim B_Q$ is moderate, $\gamma \sim 10^3$. It is far below the electron Lorentz factors that would be reached in the double layer discussed in the previous section.

After the scattering, the photon energy is boosted by a factor comparable to γ^2 , putting the originally keV photon into the GeV range, $E_{\gamma} \sim 1$ GeV. Such energetic

¹ This simple resonance condition remains valid in ultrastrong fields $B \gg B_Q$ when one takes into account the electron recoil in scattering and the fact that the target photon is propagating almost parallel to \mathbf{B} when viewed in the electron rest frame, because of the relativistic aberration effect (BT07).

gamma-rays can easily convert to e^\pm pairs in the strong magnetic field, as soon as the gamma-ray pitch angle with respect to the magnetic field, θ_γ , is large enough to satisfy the threshold condition,

$$E_\gamma \sin \theta_\gamma > 2m_e c^2. \quad (9)$$

In the region near the star where $B > 10^{13}$ G the conversion occurs practically immediately following resonance scattering (Beloborodov 2013).

The efficiency of pair creation implies a quick development of electric discharge until the number of created particles becomes sufficient to screen the accelerating electric field. The process develops in a runaway (exponential) manner and hence the accelerating voltage is unlikely to grow beyond a characteristic value that makes particles capable of resonant scattering. This condition defines a ‘‘threshold’’ for discharge, which corresponds to a characteristic electron Lorentz factor γ_{thr} .

2.3. Characteristic timescales and energy scales

The shortest timescale of interest is the plasma scale ω_p^{-1} . It describes the growth rate of the local accelerating electric field in response to charge starvation (BT07). It also determines the thickness of the surface charge c/ω_p in the double-layer configuration.

The characteristic dynamic timescale of the electric circuit is the light crossing time or the Alfvén crossing time of the system,

$$t_A = \frac{L}{c} \sim 0.3 L_7 \text{ ms}, \quad (10)$$

where L is the length of the magnetospheric field line. The group speed of Alfvén waves is always directed along the magnetic field lines and its value is close to c in the magnetically dominated corona.

The longest timescale in the problem is the lifetime of the magnetic twist. The finite voltage sustaining the magnetospheric current implies a finite ohmic dissipation rate, so the magnetic twist energy E_{twist} must dissipate with time,

$$\frac{dE_{\text{twist}}}{dt} \approx \frac{d}{dt} \int \frac{B_\phi^2}{8\pi} dV \sim I\Phi_e, \quad (11)$$

where I is electric current flowing through the magnetosphere. The voltage Φ_e controls the timescale of this evolution,

$$t_{\text{ohm}} \sim \frac{E_{\text{twist}}}{I\Phi_e}. \quad (12)$$

Using the characteristic $I \lesssim \psi(c/4\pi)BR_\star$ and $\gamma_{\text{thr}} \sim 10^3$ one can estimate that t_{ohm} is comparable to one year. This theoretical timescale for untwisting is comparable to the observed decay timescale in transient magnetars following an outburst of activity.

Because of the vast separation of timescales, $t_{\text{ohm}} \gg t_A$, the ohmic dissipation of the magnetospheric twist can be viewed as a quasi-steady process slowly draining the twist energy. Unsteadiness of the discharge may lead to strong variability in the electric circuit, however it occurs on very short timescales, which would be hard to resolve observationally.

The characteristic scales for energy (or electron Lorentz factor γ) also have an important hierarchy. The

highest energy corresponds to γ_{DL} , which would only be achieved in the absence of pair creation. It is given by Equation (6) and can exceed 10^6 . The next characteristic γ is determined by the threshold for e^\pm discharge γ_{thr} , which is comparable to 10^3 . Both γ_{DL} and γ_{thr} are much greater than unity.

2.4. Mechanism of untwisting

An integral form of the Faraday’s induction law $\partial\mathbf{B}/\partial t = -c\nabla \times \mathbf{E}$ leads to a simple equation describing resistive evolution of the axisymmetric twist (Beloborodov 2011),

$$\dot{\psi} = 2\pi c \frac{\partial\Phi_e}{\partial f}. \quad (13)$$

Here $f(r, \theta)$ is the poloidal magnetic flux function (constant along a magnetic flux surface), which serves to label the magnetic field lines. For any given point (r, θ) , f is defined as the magnetic flux through the circle about the axis of symmetry passing through the point; $f = 0$ on the axis of symmetry. In particular, for a dipole poloidal field with a dipole moment μ the flux function is given by

$$f = \frac{2\pi\mu \sin^2 \theta}{r}, \quad 0 \leq f \leq f_{\text{max}} = \frac{2\pi\mu}{R_\star}. \quad (14)$$

Note that $\sin^2 \theta/r = \text{const}$ along a dipole field line. It is convenient to use the dimensionless flux function

$$u \equiv \frac{f}{f_{\text{max}}} = \sin^2 \theta_\star, \quad (15)$$

where θ_\star is the polar angle of the magnetic field line footprint on the stellar surface.

Equation (13) shows that the twist must decrease where $\partial\Phi_e/\partial f < 0$ and increase where $\partial\Phi_e/\partial f > 0$. The fact that $\Phi_e(f_{\text{max}}) = 0$ (the field line f_{max} is confined to the star, which we approximate as an ideal conductor) implies $\partial\Phi_e/\partial f < 0$ at some $f < f_{\text{max}}$. This region with large f , comparable to f_{max} , corresponds to the inner magnetosphere near the equator, with short field lines. B09 showed that this fact leads to immediate formation of a ‘‘cavity’’ with $j = 0$ in the equatorial region near the star, and the cavity expands on the timescale t_{ohm} , erasing the magnetospheric currents. The currents are ‘‘sucked’’ into the star, so that they close inside the conductor.

From the untwisting equation it is evident that the profile of $\Phi_e(f)$ plays the key role for the twist evolution. Voltage regulated by pair discharge is expected to satisfy the condition $e\Phi_e \sim \gamma_{\text{thr}} m_e c^2$. Its variation with f over a region $\Delta f = f_{\text{max}} \Delta u$ gives the characteristic twist evolution timescale,

$$t_{\text{ohm}} = \frac{\psi}{\dot{\psi}} \sim \frac{\mu}{c\Phi_{\text{thr}}R_\star} \psi \Delta u. \quad (16)$$

The dimensionless quantities Δu and ψ are comparable to unity, and the characteristic timescale is set by the ratio μ/Φ_{thr} . Note however that t_{ohm} can strongly differ for different magnetic field lines. In particular, if there is a region with a flat dependence of $\Phi_e(f)$, $\partial\Phi_e/\partial f = 0$, then the local $t_{\text{ohm}} = \infty$ and the twist angle ψ is ‘‘frozen’’, waiting for the cavity expansion to reach the region (B09).

Another interesting implication of Equation (13) is that on some field lines the twist may *grow* as the magnetosphere untwists. In particular, a decrease of Φ_e toward the magnetic axis, $\partial\Phi_e/\partial f > 0$, leads to $\dot{\psi} > 0$. This effect will be observed in the simulations below. Together with the cavity expansion, this means that the twist relocates toward the axis with a decreasing energy E_{twist} but possibly with increasing amplitude ψ in some regions before being completely dissipated.

3. SETUP OF THE SIMULATION

3.1. Implanting the twist

Our simulation starts with a pure dipole magnetosphere, with a magnetic moment μ and no magnetic twist, $B_\phi = 0$. The twist is gradually implanted by shearing the stellar surface with a latitude-dependent angular velocity $\omega(\theta) \parallel \boldsymbol{\mu}$. The profile of $\omega(\theta)$ determines the profile of the implanted twist; we choose a profile similar to previous magnetohydrodynamic (MHD) and force-free electrodynamic (FFE) simulations of twisted magnetospheres (Mikic & Linker 1994; PBH13),

$$\omega(\theta, t) = \omega_0(t) \frac{\Theta}{\sin\theta} \exp[(1 - \Theta^4)/4], \quad (17)$$

where $\Theta = (\theta - \pi/2)/\Delta\theta_m$ and $\Delta\theta_m = \pi/4$ is a measure of the width of the sheared region. This profile gives a smooth twist that is centered at $\theta = \pi/4$ and decreases to zero at the equator. The prefactor $\omega_0(t)$ describes the rate of implanting the twist. It is smoothly increased from zero at $t = 0$ to a chosen maximum value, kept at this value for some time, and then smoothly switched off back to zero.

As long as the duration t_{shear} of the surface shear $\omega \neq 0$ is shorter than the resistive timescale of the magnetosphere, $t_{\text{shear}} \ll t_{\text{ohm}}$, ohmic dissipation may be neglected during time t_{shear} . Then the implanted twist profile is given by

$$\psi(\theta) = \int_0^{t_{\text{shear}}} \omega(\theta, t) dt. \quad (18)$$

We choose $t_{\text{shear}} = 40R_\star/c$. Then the shearing stage is sufficiently short compared with the total duration of our simulation $t_{\text{sim}} = 350R_\star/c$ but longer than or comparable to the Alfvén crossing time t_A of the sheared region, so that twist implanting is a relatively gentle process. The maximum shear angle (near $\theta = \pi/4$) is $\psi_{\text{max}} \approx 1.6$ radian in the simulations presented below.

After the twist implantation is finished, ω is kept at zero and the boundary condition at the stellar surface becomes simply a perfect static conductor. Magnetars are slow rotators, and their light cylinders $R_{\text{LC}} \gtrsim 10^4 R_\star$ are well beyond the twisted, dissipative region. The slow spinning of the star is neglected in the present paper, which corresponds to $R_{\text{LC}} = \infty$.

The implanted twist $\psi \sim 1$ is moderate and expected to result in moderate inflation of the poloidal magnetic field lines. The main effect of surface shearing is creating a strong B_ϕ in the magnetosphere. Analytical arguments (e.g. Uzdensky 2002) and FFE simulations (PBH13) show that a stronger $\psi \gtrsim 3$ will result in a global instability of the magnetosphere, which we do not intend to study in this paper and defer to future work.

3.2. Surface atmospheric layer

We start the simulation with a complete vacuum around the star and create a dense neutral atmospheric layer at the stellar surface by injecting warm electron-ion plasma at R_\star . The atmosphere scale-height h is determined by the particle injection temperature and gravity of the star. We choose a Maxwellian injection velocity with the mean value $v_0 \approx 0.1c$ and the gravitational acceleration $g = g_0/r^2$ with $g_0 = 0.5R_\star c^2$. This gives the hydrostatic scale-height

$$h \approx \frac{v_0^2}{2g_0} \approx 0.01R_\star. \quad (19)$$

This is a much thicker atmospheric layer than the magnetar would have at a surface temperature $kT \lesssim 1$ keV. However, it is sufficiently thin and still resolved by our numerical grid (see below). The characteristic time it takes to form the atmosphere is short, $t_{\text{atm}} \sim h/v_0 = 0.1R_\star/c$. Throughout the simulation particles are continually injected and absorbed by the star, sustaining a steady atmosphere at $t \gg t_{\text{atm}}$.

The injection rate is chosen high enough to ensure a high density at the base of the atmosphere,

$$n_{\text{atm}} \gg \frac{j}{ev_0}. \quad (20)$$

The density is exponentially reduced with altitude on the scale h , and steeply drops to a low value below j/ec . Therefore, in the absence of E_{\parallel} the hydrostatic plasma is not capable of conducting the electric current j required in the twisted magnetosphere.

Where the atmospheric density $n(r)$ falls below j/ec , electric field E_{\parallel} is expected to develop in response to charge starvation and lift particles from the atmosphere. The thin and dense atmospheric layer merely makes plasma available, with no special injection assumptions at the stellar surface. The numerical experiment must show how the system responds to the surface shear described in Section 3.1 and whether the induced E_{\parallel} will self-organize to conduct the magnetospheric currents that allow the twist to be implanted.

3.3. Creation of e^\pm pairs

If E_{\parallel} accelerates the lifted electrons to high Lorentz factors $\gamma > \gamma_{\text{thr}}$, pair creation will be ignited. In this paper, we use the simplest implementation of this process: we choose a fixed value for γ_{thr} and let a new e^\pm pair be instantaneously created every time an electron (or positron) reaches γ_{thr} . This may be a reasonable approximation for the e^\pm discharge near the star where $B \gg 10^{13}$ G (Beloborodov 2013). However, it becomes poor at larger distances where the magnetic field is weak and resonantly scattered photons have lower energies.

An additional simplification in our implementation is the prescription for the energy of the created pair. We will assume that the pair takes a fixed energy ΔE from the primary particle, and shares it equally, i.e. the new e^+ and e^- each receives $\Delta E/2$ (including the rest mass). Total energy and momentum parallel to \mathbf{B} is conserved in the pair creation process.

Thus, we do not track the propagation of any high-energy photons, which is significantly simpler than the discharge model of CB14 developed for pulsars. The

simplified version appears adequate for the first axisymmetric PIC model of magnetars. It should be sufficient to demonstrate some basic features of plasma self-organization in response to shearing of the magnetospheric footpoints, followed by ohmic dissipation of the twist. The results may be used as a benchmark for future more advanced simulations. Future simulations will have explicitly implemented resonant scattering process, so that ΔE will be the energy of the resonantly scattered photon, which may convert to e^\pm with a delay. Both γ_{thr} and ΔE will vary with the local magnetic field, see Beloborodov (2013) for a detailed discussion.

3.4. Rescaling of large numbers in the problem

Any PIC simulation must resolve the plasma skin depth $\lambda_p = c/\omega_p$, which is a demanding condition on the computational grid, as λ_p is a microscopic scale and the ratio R_\star/λ_p is huge (comparable to 10^8 in magnetars). Similar to the PIC simulations of rotation-powered pulsars, this issue is resolved by rescaling the parameters of the problem so that λ_p remains much smaller than the stellar radius, $\lambda_p \sim 10^{-2}R_\star$, but becoming sufficiently large to be well resolved. This rescaling has two main implications:

(1) Similar to the pulsar problem, the increased λ_p implies a reduction of the energy scales (cf. CB14). In particular, the maximum voltage that can be induced in a magnetar magnetosphere is given by γ_{DL} (Equation 6), which now becomes moderate, $\gamma_{\text{DL}} \sim 10^2$. To respect the hierarchy of the energy scales $1 \ll \gamma_{\text{thr}} \ll \gamma_{\text{DL}}$, a good choice for the discharge threshold in the numerical experiment is $\gamma_{\text{thr}} \sim 10$. Secondary pairs receive the energy ΔE , which must be a fraction of $\gamma_{\text{thr}}m_e c^2$. We will fix $\Delta E = 3.5m_e c^2$ for all simulations presented below.

(2) The rescaling of λ_p changes the lifetime of the implanted twist, as seen from the following estimate. The value of $\lambda_p = c/\omega_p$ is related to the electric current density j by Equation (3), and the characteristic value of j scales with the magnetic dipole moment of the star μ : $j \sim \psi (c/4\pi)(\mu/R_\star^4)$. This gives,

$$\left(\frac{\lambda_p}{R_\star}\right)^2 \sim \frac{m_e c^2 R_\star^2}{e\mu\psi}. \quad (21)$$

Combining this relation with Equation (16) for the resistive evolution timescale, one obtains

$$t_{\text{ohm}} \sim \gamma_{\text{thr}}^{-1} \left(\frac{R_\star}{\lambda_p}\right)^2 \frac{R_\star}{c}. \quad (22)$$

One can see that the rescaling of λ_p to $\sim 10^{-2}R_\star$ reduces the resistive timescale to $t_{\text{ohm}} \sim 10^3(R_\star/c)$ when $\gamma_{\text{thr}} \sim 10$. This is fortunate, as the untwisting evolution can now be observed during a reasonably long simulation. With the realistic $\lambda_p/R_\star \sim 10^{-8}$ and $\gamma_{\text{thr}} \sim 10^3$ one would have $t_{\text{ohm}} \sim 10^{13}R_\star/c$.

Another large number that should be rescaled in the simulation is the ion-to-electron mass ratio $m_i/m_e \approx 2 \times 10^3$. We use $m_i/m_e = 10$. This rescaling is useful for two reasons: (1) The characteristic ion plasma frequency $\omega_{p,i} = (4\pi n_i e^2/m_i)^{1/2}$ is not very much smaller than ω_p , so that $\omega_{p,i} < r/c$ is well satisfied, and (2) $m_i c^2$ becomes

comparable to $\gamma_{\text{thr}}m_e c^2$. The latter coincidence is also expected for the real magnetar discharge.

It is also useful to evaluate the surface magnetic field $B_\star \sim \mu/R_\star^3$, which can be expressed from Equation (21), and then estimate the characteristic gyro-frequency,

$$\omega_B = \frac{eB_\star}{m_e c} \sim \frac{c}{R_\star} \left(\frac{R_\star}{\lambda_p}\right)^2, \quad (23)$$

where λ_p corresponds to the current density supporting a twist $\psi \sim 1$. One can see that the particles are very strongly magnetized, $\omega_B \sim 10^4 c/R_\star$, and hence expected to move along the magnetic field lines, similar to real magnetars. The characteristic gyro-frequency is also related to another important parameter of the magnetosphere — the ratio of magnetic and plasma energy densities,

$$q = \frac{B^2}{4\pi\gamma n m_e c^2} = \frac{\omega_B^2}{\gamma\omega_p^2}. \quad (24)$$

For real parameters of magnetars this ratio is $q \sim 10^{17}$. The characteristic parameters chosen in our simulations give $q \sim 10^3$. This is still very much above unity, so the magnetosphere is nearly force-free as it should be.

The parameter q also determines the Lorentz factor of Alfvén waves, $\gamma_A \approx q^{1/2}$. For a real magnetar, this gives $\gamma_A \gg \gamma \sim \gamma_{\text{thr}}$. This condition is satisfied in our rescaled numerical experiment as long as $\gamma_{\text{thr}} \ll 30$.

3.5. Evolving the fields and the plasma: Aperture

The particle-in-cell (PIC) method provides an efficient technique to simulate plasma from first principles. The electromagnetic fields are evolved on a grid according to Maxwell equations with the source (electric current and charge density) provided by the plasma that is self-consistently evolved in the electromagnetic field. The plasma is represented directly as a large number of individual particles. The simulation follows the motion of each particle by calculating the applied forces. The motion of the plasma particles creates electric current which is interpolated onto the grid and then used as the source term in the Maxwell equations to update the electromagnetic field. The method well describes the plasma behavior at the microscopic kinetic level as long as the plasma skin depth is well resolved by the grid and the number of particles per grid cell is much larger than one.

Our simulations are performed using the PIC code Aperture.² The code was originally developed for the PIC simulations of rotationally powered pulsars (CB14). The code can follow pair creation with or without explicit tracking of high-energy photons. In the present work we use the simplified implementation of pair creation (Section 3.3) and do not use the radiative transfer module. The code is fully relativistic and designed to work on curvilinear grids. This is particularly important for problems with natural spherical geometry, such as the plasma dynamics around a spherical star in a region extending far beyond the stellar radius.

The simulations presented below are done in 2.5D, which means that our grid is 2D (in the poloidal plane)

² Aperture is a recursive acronym: Aperture is a code for Particles, Electromagnetic fields, and Radiative Transfer at Ultra-Relativistic Energies.

but all vector quantities are fully 3D, and we solve the full Maxwell equations assuming axisymmetry. Particles in the simulation may be thought of as rings with poloidal and toroidal velocity components. We use a spherical r, θ grid with logarithmic spacing in r and uniform spacing in θ . For all of the simulations shown in this paper, the grid size is 384×384 and the timestep $\Delta t = 10^{-3} R_\star/c$.

The outer boundary of the simulation box is set at $r_{\text{out}} = 30R_\star$ and employs a damping condition that lets outgoing electromagnetic waves and particles escape the box, preventing reflection. We did not detect any appreciable reflection of waves from the outer boundary. Note also that most of the active (current carrying) field lines are closed well inside the box and do not cross the outer boundary.

The shear motion of the stellar surface during the twist implantation stage $t < t_{\text{shear}} = 40R_\star/c$ is equivalent to imposing a tangential electric field at the boundary. The field corresponding to the surface motion with velocity \mathbf{v} in the lab frame is given by $\mathbf{E} = -\mathbf{v} \times \mathbf{B}/c$. It corresponds to zero electric field in the comoving frame of the stellar crust, which is assumed to be an ideal conductor. This gives the following boundary condition at $r = R_\star$,

$$\mathbf{E}(t, \theta) = -\frac{(\boldsymbol{\omega}(t, \theta) \times \mathbf{r}) \times \mathbf{B}}{c}. \quad (25)$$

The initial state is a dipole field and the normal component of the magnetic field at the surface remains unchanged during the simulation.

3.6. Units

A set of natural units can be defined as follows. All lengths are measured in units the stellar radius R_\star and time is measured in R_\star/c . The corresponding velocity unit is the speed of light c . We define the dimensionless electromagnetic field and current density as

$$\tilde{E} = \frac{eR_\star E}{m_e c^2}, \quad \tilde{B} = \frac{eR_\star B}{m_e c^2}, \quad \tilde{j} = \frac{4\pi e R_\star^2 j}{m_e c^3}. \quad (26)$$

Hereafter we will use tilde to denote dimensionless quantities, e.g. $\tilde{r} = r/R_\star$, $\tilde{t} = ct/R_\star$ etc.

4. RESULTS

In all simulations presented below the magnetic field strength at the pole of the star is $\tilde{B}_{\text{pole}} = 4 \times 10^4$. It corresponds to $\tilde{\omega}_B = 4 \times 10^4$. We focus on the simulation with $\gamma_{\text{thr}} = 10$, as it gives the best re-scaled model of real magnetars (Section 3.4). Simulations with different γ_{thr} are only discussed in Section 4.3.

4.1. Initial relaxation

During the initial stage of the simulation $\tilde{t} < \tilde{t}_{\text{shear}} = 40$ the dipole magnetosphere is twisted by the surface shearing motion described in Section 3.1. The surface motion induces a parallel electric field E_{\parallel} , which lifts charges from the atmospheric layer into the magnetosphere and accelerates them. The electron Lorentz factors quickly reach γ_{thr} and e^\pm discharge is triggered within a single Alfvén time of the twisted field line bundle.

The e^\pm plasma created by the discharge screens E_{\parallel} , and the voltage along the current loop temporarily drops,

shutting down the discharge. As the created pairs are lost to the star on the light-crossing time, a charge-starved region with significant E_{\parallel} develops again. This first happens near the equatorial plane. As a result, an equatorial gap with strong E_{\parallel} emerges and begins to accelerate particles, sustaining the pair creation process. The gap structure and how the e^\pm discharge is sustained will be described in more detail in Section 4.2.

It is clear from the simulation that a magnetospheric source of pair plasma is established in the twisted magnetosphere on a timescale not much longer than the light crossing time, before the surface shearing ends at t_{shear} . Pair creation becomes the dominant source of plasma; the extraction of particles from the atmospheric layer is only important at the initial stage igniting the e^\pm discharge. After the pair discharge is activated, only a small fraction of the magnetospheric current is carried by the particles lifted from the surface. In particular, we observed that less than 1% of the current is carried by the ions.

We also observed that the twist implantation at $t < t_{\text{shear}}$ is accompanied by excitation of Alfvén waves, which bounce back and forth along the magnetospheric field lines.³ Similar waves were observed in FFE simulations (PBH13). The waves are damped in the magnetosphere at later times, and the initial relaxation period is followed by the gradual evolution on a much longer timescale $\tilde{t}_{\text{ohm}} \gg 100$.

After the surface shearing stopped at t_{shear} , the electric discharge persisted for the rest of the simulation. It continually supported the electric current in the slowly untwisting magnetosphere, and the created particles continually bombarded the star. The duration of the simulation $\tilde{t}_{\text{sim}} = 350$ was approximately 9 times longer than t_{shear} and comparable to the expected resistive timescale \tilde{t}_{ohm} estimated in Section 2. The observed gradual evolution of the magnetospheric twist and currents on the timescale $\sim \tilde{t}_{\text{ohm}}$ will be described in Section 4.4.

4.2. The equatorial gap

A key aspect of the discharge self-organization is how and where particles are accelerated. The simulation clearly shows the formation of a quasi-steady “gap” with a strong E_{\parallel} concentrated around the equatorial plane (Figure 1). The gap thickness ℓ_{gap} is smaller than radius, and its voltage is near the threshold for e^\pm discharge,

$$\Phi_{\text{gap}} \approx \ell_{\text{gap}} E_{\text{gap}}, \quad e\Phi_{\text{gap}} \approx \gamma_{\text{thr}} m_e c^2. \quad (27)$$

Particles are accelerated in the gap and most of the pair creation events happen around this region.

As seen in Figure 1, the gap has a rather sharp boundary; E_{\parallel} is screened outside it by the created e^\pm plasma. The drop of E_{\parallel} across the two boundaries of the gap is sustained by the layers of positive and negative charge ($\pm \Sigma$ above and below the equatorial plane, respectively), according to Gauss law $\nabla \cdot \mathbf{E} = 4\pi\rho$. The charged layers are self-consistently sustained by the difference in velocities of positive and negative charges passing through them in the self-organized E_{\parallel} .

³ Alfvén waves are reflected from the rigid sphere and trapped in the magnetosphere. Our simulation neglects the fact that the crustal material has a finite strength, which can lead to plastic damping of Alfvén waves in the crust (Li & Beloborodov 2015).

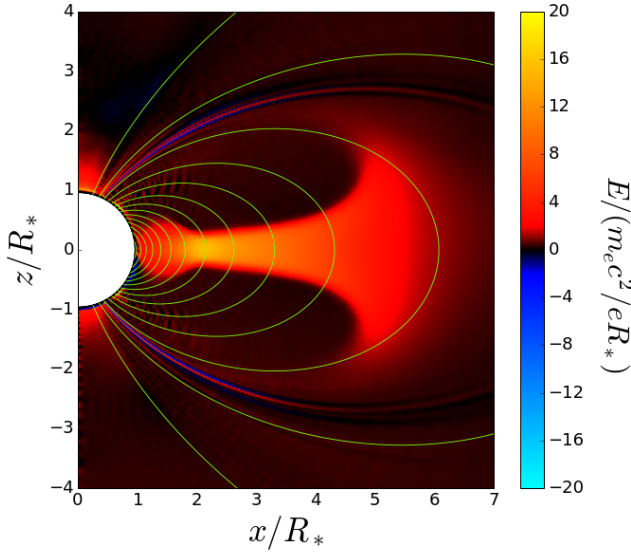


Figure 1. Electric gap in the twisted magnetosphere. Magnetic field lines are shown by the green curves (poloidal cross section), and color shows the parallel electric field, defined as $E_{\parallel} = \mathbf{E} \cdot \mathbf{B}/B$, in our standard units defined in Section 3.6. The plot shows the average of a series of snapshots centered around $\tilde{t} = 200$. The gap voltage is self-regulated to the discharge threshold γ_{thr} ; $\gamma_{\text{thr}} = 10$ in the simulation.

In essence, the gap is a double layer. It has been compressed toward the equatorial plane to a minimum thickness ℓ_{gap} that is still capable of sustaining particle acceleration to γ_{thr} . Similar to the double layer described in Section 2.1, the charge layers sandwiching the gap have the thickness comparable to the local plasma skin depth λ_p (evaluated for charge density $\sim j/c$) (Figure 2). The electric field in the gap is $E_{\text{gap}} \sim 4\pi(j/c)\lambda_p$ and its voltage is

$$e\Phi_{\text{gap}} \sim \frac{\ell_{\text{gap}}}{\lambda_p} m_e c^2. \quad (28)$$

The self-regulation of the gap voltage to $\Phi_{\text{gap}} \approx \Phi_{\text{thr}}$ controls the gap thickness $\ell_{\text{gap}} \sim \gamma_{\text{thr}} \lambda_p$.

Unlike normal double layers, particles accelerated in the gap are not brought from outside; instead, the gap feeds itself with particles. The accelerated particles create secondary e^{\pm} of lower energies near the gap exit, and some of the secondary particles are reversed by E_{\parallel} and accelerated toward the opposite boundary of the gap, where they create new pairs, etc.

The multiplicity of the pair plasma is defined by $\mathcal{M} = (\rho_+ - \rho_-)/j$, where ρ_+ and ρ_- are the charge densities of the positrons and electrons, respectively. One can see in Figure 3 that \mathcal{M} in the gap is close to 1, i.e. the gap contains the minimum amount of plasma needed to conduct the electric current. This is consistent with no screening in the gap that allows the strong E_{\parallel} to be sustained. Pair multiplicity in other parts of the j-bundle is close to 2, just sufficient to screen E_{\parallel} . Apparently, the discharge in the simulation is self-organized to carry the current with the minimum voltage $\Phi_e \approx \Phi_{\text{gap}} \approx \Phi_{\text{thr}}$ and the minimum rate of pair creation.

Figure 4 shows the average hydrodynamic momenta of electrons and positrons. It is apparent that both species

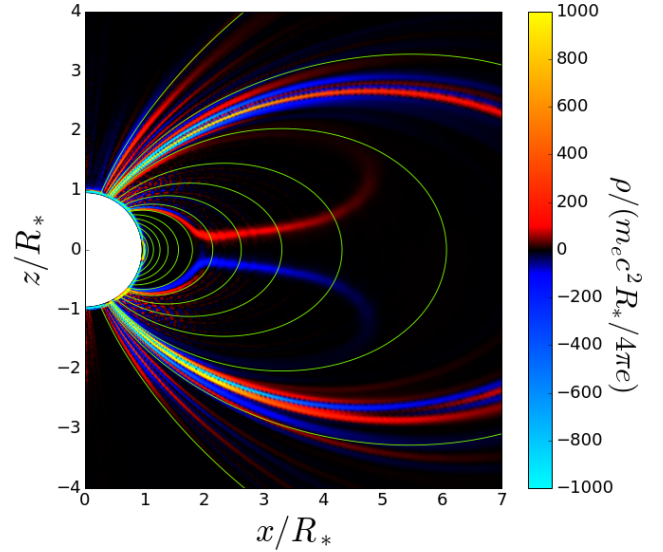


Figure 2. Charge density in the magnetosphere, averaged in the same way as in Figure 1. Note the thin charged layers bounding the equatorial gap across the magnetic field lines. The layers extend into the inner magnetosphere along the inner boundary of the j-bundle. The charged structure observed on the field lines extending to $\tilde{r} \sim 9$ approximately corresponds to the outer boundary of the j-bundle (see Figure 6).

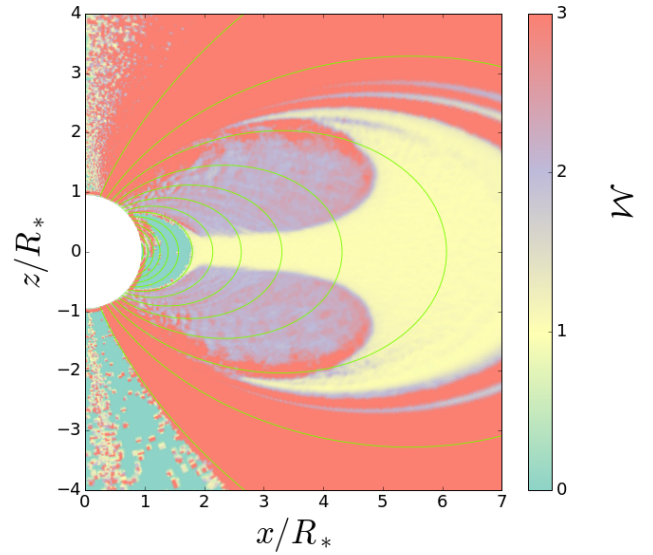


Figure 3. Pair multiplicity $\mathcal{M} = (\rho_+ - \rho_-)/j$.

are accelerated across the equatorial gap to the threshold Lorentz factor $\gamma_{\text{thr}} = 10$. The move with almost speed of light in the opposite directions and make approximately equal contributions to the current density, consistent with $\mathcal{M} \approx 1$. Outside the gap, $\mathcal{M} \approx 2$ together with the charge neutrality condition $n_+ \approx n_-$ implies that the current is carried by one species while the other creates the neutralizing, nearly static, background. This is indeed observed in Figure 4.

The gap voltage is not exactly steady and shows quasi-

periodic “breathing” with time. This must assist the gap in reversing some of the secondary particles so that they can cross the gap and accelerate to γ_{thr} , sustaining the pair creation cycle. Most of the accelerated particles escape the gap and get absorbed by the star.

Since the magnetosphere was set up to be symmetric about the equatorial plane, the fact that the current is strongly dominated by created pairs implies symmetric bombardment of the two footprints of the j-bundle. Thus, our simulation shows two symmetric hot spots (or rather rings, due to the axial symmetry) in the northern and southern hemispheres of the star.

As discussed in BT07 and Section 2.1, the voltage Φ_e in the magnetospheric circuit is purely inductive. The parallel electric field $\mathbf{E} = -c^{-1}\partial\mathbf{A}/\partial t$ is associated with the slow dissipation of B_ϕ rather than an electrostatic potential. Note also that the dissipation rate $\mathbf{E}\cdot\mathbf{j} = E_{\parallel}j$ is localized in the gap while the untwisting of B_ϕ also occurs outside the gap. The re-distribution of the dissipated B_ϕ along the j-bundle into the screened region with $E_{\parallel} \approx 0$ occurs through the Alfvén mode, which can propagate without dissipation. The Alfvén timescale $t_A \sim r/c$ is much shorter than the untwisting timescale t_{ohm} , and so the magnetosphere slowly evolves through the sequence of global twist equilibria of a decreasing energy E_{twist} , even though the magnetic energy is converted to heat only near the equator.

4.3. Dependence on the threshold voltage

While the simulation with $\gamma_{\text{thr}} = 10$ is the most adequate re-scaled version of the magnetar magnetosphere (Section 3.4), we also performed simulations with $\gamma_{\text{thr}} = 20, 100,$ and ∞ (no pair creation). All other parameters of the four simulations were identical.

Figure 5 shows the evolution of the twist energy E_{twist} in the simulations with the four different values of γ_{thr} . An obvious trend is observed: a higher threshold voltage for discharge, $e\Phi_{\text{thr}} = \gamma_{\text{thr}}m_e c^2$, leads to a higher dissipation rate and a shorter lifetime of the magnetic twist. When $\gamma_{\text{thr}} \gg 10$, the dissipation becomes so strong that it affects the initial stage of the twist implantation at $\tilde{t} < \tilde{t}_{\text{shear}} = 40$, so that a substantial part of the twist amplitude (and the corresponding energy E_{twist}) is lost before it could be implanted.

The extreme model with $\gamma_{\text{thr}} = \infty$ gives so strong dissipation that E_{twist} does not reach even 10% of its target value. It is instructive to compare this simulation with the expected dissipation rate in the pair-free configuration described in Section 2.1. From equation (6), we can estimate the voltage drop of the double layer as $\gamma_{\text{DL}} = \tilde{\Phi}_e \sim \sqrt{\tilde{j}}\tilde{W}$. The initial width of the j-bundle near the star is $\tilde{W} \sim 1$. The target current density reaches $\tilde{j} \sim 3 \times 10^4$ if the twist is fully implanted. This estimate gives γ_{DL} comparable to 200; the actual voltage in the simulation reaches somewhat higher values. The high voltage develops early during the shearing stage and results in strong dissipation, which does not allow \tilde{j} to approach 3×10^4 .

The simulation with $\gamma_{\text{thr}} = 100$ enables the pair discharge, which buffers the voltage growth in the j-bundle and allows a stronger twist to be implanted. The simulations with $\gamma_{\text{thr}} = 20$ and, in particular, $\gamma_{\text{thr}} = 10$, allow almost full implantation of the target twist with

small ohmic losses. The subsequent slow resistive evolution is similar in the two models, as both have Φ_{thr} well below the double-layer voltage and sustain a long-lived discharge activity in the j-bundle. As expected, the untwisting timescale t_{ohm} is reduced by a factor of 2 as γ_{thr} is increased from 10 to 20 (see Equation 16).

These results unambiguously demonstrate that the energy dissipation timescale is controlled by the pair creation threshold, confirming the conclusion of BT07. In real magnetars, we expect $\gamma_{\text{thr}} \ll \gamma_{\text{DL}}$ (Section 2). Therefore, the most relevant model is the one with low $\gamma_{\text{thr}} = 10$, which is still high enough to accelerated particles to ultra-relativistic energies and produce relativistic secondary e^\pm .

4.4. Expanding cavity

Figure 6 shows the resistive evolution of the j-bundle. The untwisting of the magnetic field lines proceeds as anticipated in Section 2.4, through formation of a cavity $j = 0$ that expands from the inner magnetosphere near the equator (large flux function u). Figure 7 shows the evolution of the poloidal current j_p until the end of the simulation at $\tilde{t}_{\text{sim}} = 350$. We chose to show j_p/B_p because this quantity is constant along the magnetic field lines (after averaging over short-timescale fluctuations), as expected in a nearly force-free magnetosphere — currents flow along the magnetic field lines. Therefore, j_p/B_p is a function of the magnetic field line, which we label by the parameter $u = \sin^2\theta_*$ (see Equation 15). Note the expansion of the region where $j_p = 0$ toward the magnetic axis, from $u \approx 0.75$ to $u \lesssim 0.55$.

Figure 8 shows the evolution of the integrated twist angle ψ defined in Equation (1). The untwisting proceeds from near the equator, where the twist angle decreases over time, but the twist angle is not simply erased, but relocated from the inner magnetosphere to the outer parts, as expected from the untwisting Equation (13).

A curious feature is observed to develop on the magnetic field lines with u around 0.22: the twist angle ψ grows and approaches 3.5 toward the end of the simulation. This feature is also seen in the current structure shown in Figures 6 and 7. The strongly twisted, narrow bundle of field lines is inflating with time and eventually opens up, causing a magnetospheric instability (cf. PBH13). Our simulation stopped right at the onset of this development, since we would like to limit our study to the quasi-steady untwisting regime. An important difference from over-twisting studied in PBH13 is that here it is not driven by excessive surface shear. Instead, it results from resistive evolution of the implanted twist while the crust is static.

5. DISCUSSION

We have performed the first axisymmetric particle-in-cell simulations of the twisted magnetospheres of magnetars. The simulations demonstrate from first principles that electric e^\pm discharge is self-organized in the magnetosphere to sustain the electric current j demanded by the magnetospheric twist.

The results of our numerical experiment may be summarized as follows.

1. Shear motion of the stellar surface on a timescale $t_{\text{shear}} < t_{\text{ohm}}$ successfully implants a magnetic twist

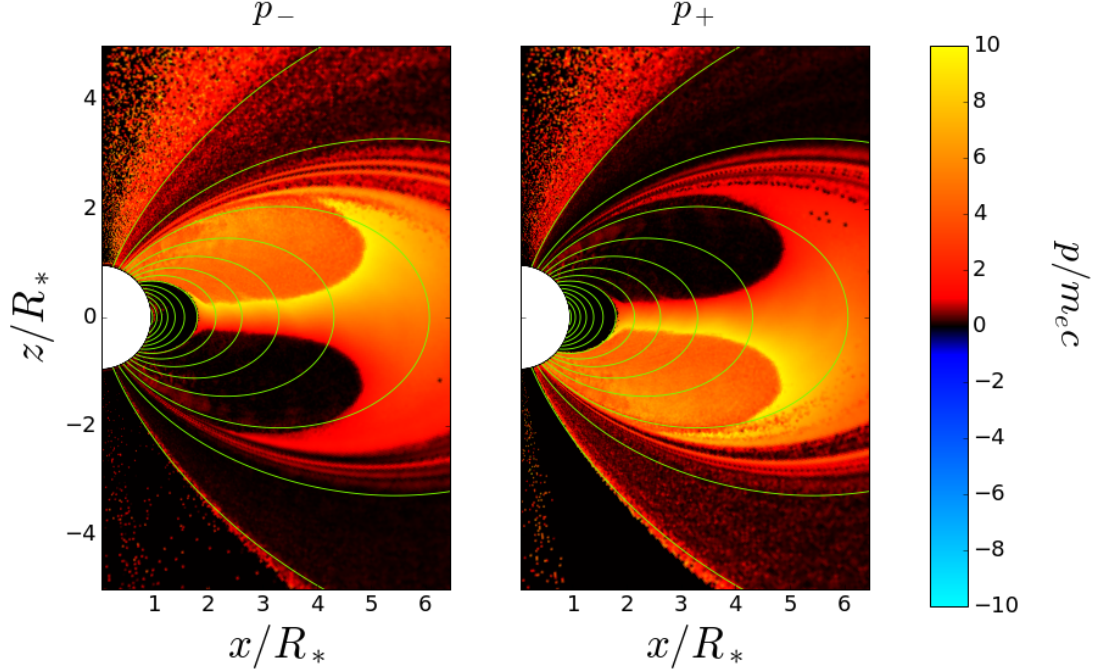


Figure 4. Average hydrodynamic momentum of electrons (left) and positrons (right).

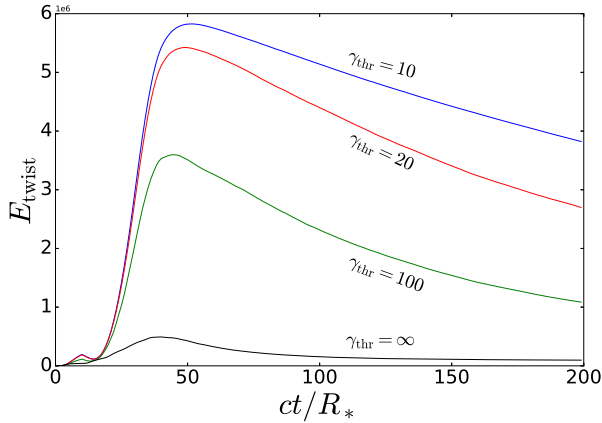


Figure 5. Evolution of the twist magnetic energy E'_{twist} . Four simulations are shown with discharge thresholds $\gamma_{\text{thr}} = 10, 20, 100, \infty$. We use the exact expression for $E'_{\text{twist}} = \int (B^2 - B_0^2)/8\pi dV$, where B_0 is the initial dipole field. It takes into account that besides $B_\phi^2/8\pi$ part of the twist energy is stored in the inflated poloidal magnetic field, which becomes important when the twist amplitude ψ exceeds unity.

- in the magnetosphere. The twist is supported by continual electric current due to self-organized e^\pm discharge.
- Particles are accelerated along the magnetic field lines to Lorentz factors $\gamma \approx \gamma_{\text{thr}}$, just sufficient to ignite pair creation. The voltage sustaining the electric circuit, the dissipation rate, and the lifetime of the twist are all regulated by γ_{thr} .
 - Particle acceleration is localized in a gap near the equatorial plane (Figure 1). The gap has the electric field $E_{\parallel} \sim 4\pi(j/c)\lambda_p$ and width $\ell_{\text{gap}} \sim \gamma_{\text{thr}}\lambda_p$, where $\lambda_p = (m_e c^3/4\pi e j)^{1/2}$ is the local plasma

skin-depth. The plasma density in the gap is close to the minimum value $n = j/ec$ required to conduct the electric current. Continual e^\pm creation occurs near the two exits from the gap.

- The magnetospheric current is carried by electrons and positrons created in the magnetosphere rather than electrons and ions extracted from the atmospheric layer on the stellar surface. The created particles rain onto the footprints of the j -bundle, creating two hot spots.
- Resistive untwisting of the magnetosphere occurs on the timescale t_{ohm} estimated in Equation (16), in agreement with theoretical expectations. The evolution proceeds as predicted in B09: a cavity with $j = 0$ quickly forms in the inner magnetosphere and gradually expands, erasing the remaining electric currents.
- A curious feature was observed in the untwisting process: while the twist energy was decreasing as expected from ohmic dissipation, the twist amplitude ψ grew in a narrow bundle of field lines at the outer boundary of the twisted region. This over-twisted bundle inflated so much that it eventually opened up.

Our results confirm that the untwisting magnetospheres naturally create shrinking hot spots (footprints of the shrinking j -bundle), which have been detected in 7 transient magnetars. The evolution timescale inferred from the simulations (Equation 16) is consistent with the decay timescale observed in transient magnetars (months to years).

One unknown in the setup of our numerical experiment is the profile of the surface shear. However, basic features observed in the simulation, in particular voltage

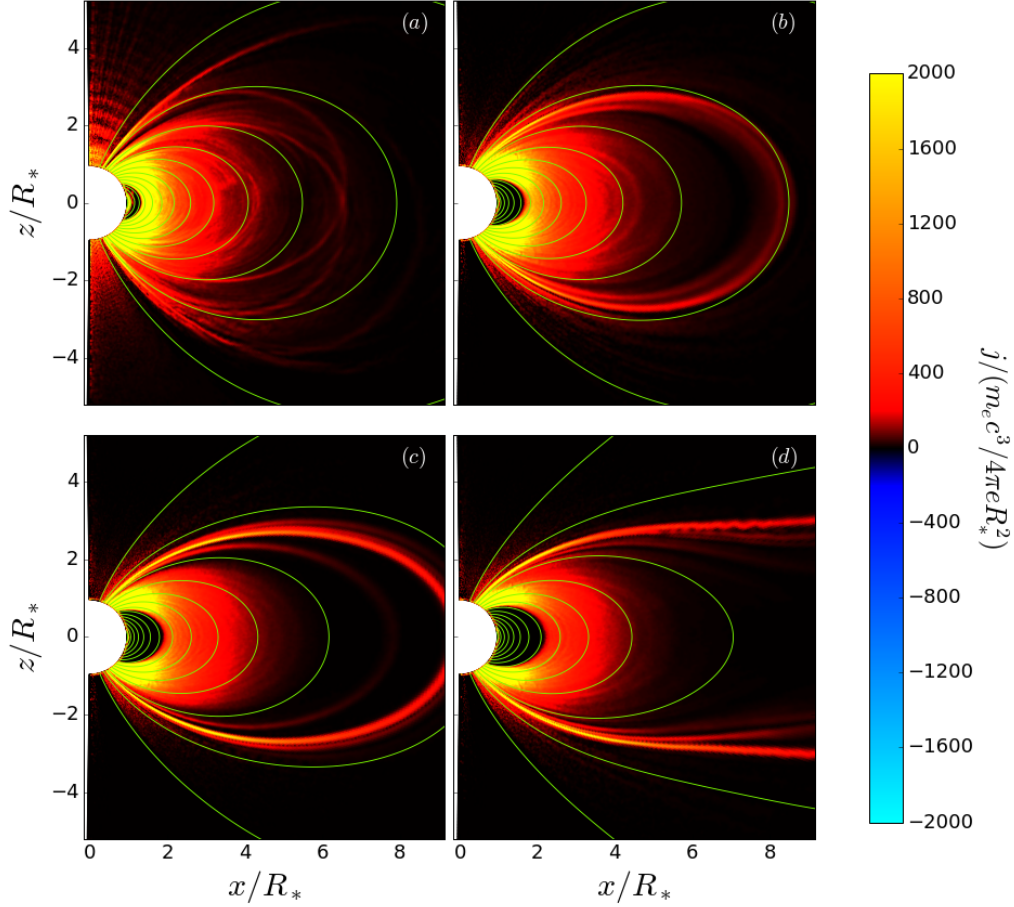


Figure 6. Color plot showing the evolution of the poloidal current density j_p in the simulation with $\gamma_{\text{thr}} = 10$. Four snapshots are shown: (a) $\tilde{t} = 30$, (b) $\tilde{t} = 120$, (c) $\tilde{t} = 230$, and (d) $\tilde{t} = 350$. Note that when $j_p = 0$ then also $j = 0$.

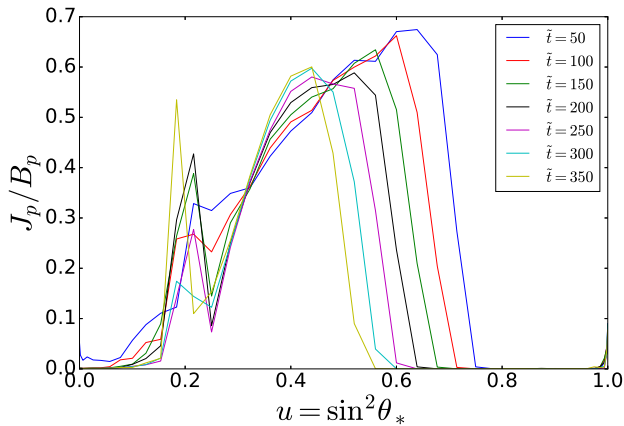


Figure 7. Evolution of the poloidal current distribution in the magnetosphere in the simulation with $\gamma_{\text{thr}} = 10$. The ratio j_p/B_p (constant along the magnetic field lines) is shown versus the poloidal flux function defined in Equation (15); θ_* is the polar angle of magnetic field line footprint on the star. The different curves show snapshots at times $\tilde{t} = 50, 100, 150, 200, 250, 300$, and 350.

regulation through e^\pm discharge and the cavity expansion, should be generic and independent of the details of the twist profile. It is less clear how generic is the formation of the narrow over-twisted bundle. This could

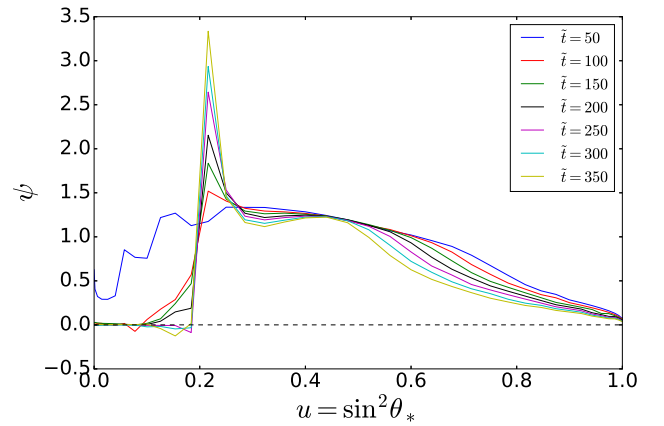


Figure 8. Evolution of the twist angle ψ in the simulation with $\gamma_{\text{thr}} = 10$.

be further explored with simulations of different shear profiles.

An important caveat in the simulation setup is the simplified “on the spot” prescription for pair creation, with the created e^\pm pair taking a significant energy fraction from the primary particle. As briefly discussed in Section 3.3, this prescription is reasonable if the twist is confined to the region of ultrastrong magnetic field near

the star, $B \gtrsim B_Q$. Pair creation in weaker fields tends to occur with high multiplicities, which can launch a dense e^\pm outflow and efficiently screen E_{\parallel} in the equatorial region (Beloborodov 2013). Then the gap may have to split into two gaps and move away from the equator, closer to the star.

How the discharge will self-organize in this case can only be explored using a more detailed implementation of the pair creation process. The future simulation will directly track the high-energy photons produced by resonant scattering and their conversion to pairs, without prescribing any γ_{thr} . This will be the focus of our future work, and we expect it to establish the gap location on magnetic field lines extending far from the star. This part of the magnetosphere is interesting for two reasons: (1) the j-bundle activity tends to concentrate on the extended field lines, and (2) the nonthermal emission is able to escape the outer magnetosphere while almost all resonantly scattered photons in the region $B \gg 10^{13}$ G convert to pairs (Beloborodov 2013). Gap location on the extended field lines influences the hard X-ray spectrum emitted by the twisted magnetosphere, and thus can be tested against observations. Phase-resolved hard X-ray spectra have been measured for several magnetars and fitted by the e^\pm outflow model (e.g. Hascoët et al. 2014; An et al. 2015), which assumes an electric gap near the star. Direct PIC simulations of the e^\pm discharge of high multiplicity can verify or disprove this assumption.

We did not study in this paper what happens when the magnetosphere is over-twisted and becomes unstable. This phenomenon is associated with the observed giant flares of magnetars, an extreme analogy of solar flares. The over-twisted magnetosphere inflates and creates a thin current sheet separating magnetic fluxes of opposite polarities. The current sheet becomes unstable to the tearing mode, which leads to magnetic reconnection and ejection of plasmoids from the magnetosphere (Lyutikov 2003; PBH13), resembling the mechanism of coronal mass ejections from the sun (e.g. Mikic & Linker

1994). Our preliminary studies using Aperture show similar behavior. One difficulty encountered by such simulations is the huge pair creation rate in the dissipative current sheet, which must result in quick thermalization of the released magnetic energy. A scheme describing this transition needs to be developed and will be a topic for future work.

This work was supported by NASA grant NNX13AI34G and a grant from the Simons Foundation (#446228, Andrei Beloborodov). Some of our simulations were run on the HPC cluster Yeti at Columbia University.

REFERENCES

- An, H., Archibald, R. F., Hascoët, R., et al. 2015, *ApJ*, 807, 93
 Beloborodov, A. M., & Thompson, C. 2007, *ApJ*, 657, 967
 Beloborodov, A. M. 2009, *ApJ*, 703, 1044
 Beloborodov, A. M. 2011, *Astrophysics and Space Science Proceedings*, 21, 299
 Beloborodov, A. M. 2013, *ApJ*, 762, 13
 Beloborodov, A. M., & Levin, Y. 2014, *ApJ*, 794, L24
 Beloborodov, A. M., & Li, X. 2016, arXiv:1605.09077
 Belyaev, M. A. 2015, *MNRAS*, 449, 2759
 Carlqvist, P. 1982, *Ap&SS*, 87, 21
 Cerutti, B., Philippov, A. A., & Spitkovsky, A. 2016, *MNRAS*, 457, 2401
 Chen, A. Y., & Beloborodov, A. M. 2014, *ApJ*, 795, L22
 Goldreich, P., & Julian, W. H. 1969, *ApJ*, 157, 869
 Hascoët, R., Beloborodov, A. M., & den Hartog, P. R. 2014, *ApJ*, 786, L1
 Li, X., Levin, Y., & Beloborodov, A. M. 2016, arXiv:1606.04895
 Li, X., & Beloborodov, A. M. 2015, *ApJ*, 815, 25
 Lyutikov, M. 2003, *MNRAS*, 346, 540
 Mereghetti, S. 2008, *A&A Rev.*, 15, 225
 Mikic, Z., & Linker, J. A. 1994, *ApJ*, 430, 898
 Parfrey, K., Beloborodov, A. M., & Hui, L. 2013, *ApJ*, 774, 92
 Philippov, A. A., Spitkovsky, A., & Cerutti, B. 2015, *ApJ*, 801, L19
 Thompson, C., & Duncan, R. C. 1995, *MNRAS*, 275, 255
 Thompson, C., Lyutikov, M., & Kulkarni, S. R. 2002, *ApJ*, 574, 332
 Turolla, R., Zane, S., & Watts, A. L. 2015, *Reports on Progress in Physics*, 78, 116901
 Uzdensky, D. A. 2002, *ApJ*, 574, 1011